Determining the Functions of eIF3 in Yeast Canonical Translation Initiation

Michelle Zhou

Swastik De and Joachim Frank

Frank Lab

Abstract

Canonical translation initiation in yeast requires the coordination of multiple eukaryotic initiation factors (eIFs) with 40S and 60S ribosomes. Eukaryotic initiation factor 3 (eIF3) is essential for the assembly of the 43S PIC, the binding of mRNA to the eIF4F complex, and scanning and AUG recognition (Pestova, 2002). However, the roles of each subunit of yeIF3 (a/b/c/i/g) during yeast canonical translation initiation in the 43S PIC are unknown, as there is a lack of structural information about its location and interactions within the 43S PIC.

A novel technique allowed us to purify each subunit separately to determine how yeIF3a/c/b/i/g binds and interacts in the 43S PIC. We have analyzed a modular multicomponent system by collecting and analyzing datasets for elF3entry (aCTD/b/i/g), elF3full (a/c/b/i/g), eIF3a/c/b, and eIF3b/i/g. Gel-based assays were performed to assess eIF3's role in PIC formation and mRNA recruitment. Cryo-EM single particle analysis methods were used for structural analyses. Finally, cryoDRGN heterogeneity analysis was conducted to determine how individual eIF3 subunits influence 40S head and body dynamics.

We have determined how yeIF3a/c/b/i/g binds and interacts during yeast canonical translation initiation. In the eIF3full dataset, eIF3b/i/g binds to both sides of the 40S subunit. In the eIF3entry dataset, eIF3b/i/g is present on both sides of the 40S subunit and can bind to the 40S ribosome without eIF3a/c. The eIF3b/i/g dataset has neither eIF3a/c nor eIF3aCTD, so eIF3b/i/g poorly binds to the 40S subunit. In the eIF3a/c/b dataset, eIFb binds to the 40S subunit without eIF3i/g. Additionally, eIF3a/c stabilizes the head of the 40S. Finally, eIF3full is proficient in both PIC binding and mRNA recruitment; eIFentry can do both PIC binding and mRNA recruitment, albeit very slowly; and eIF3a/c/b is proficient in PIC binding but inactive in mRNA recruitment.

Our novel findings inform of previously unknown functions regarding yeIF3 in the 43S PIC. They show how the coordinated interaction of eIF3 subunits with the 40S ribosome supports efficient initiation. Our findings provide a robust framework for understanding how each module contributes to the overall translation mechanism. This modular mechanism model, supported by structural and biochemical data, comprehensively explains how eIF3's independent yet cooperative subunit interactions guide 43S PIC assembly and mRNA recruitment. As the most complex translation initiation factor, understanding the structure and functions of eIF3 is essential to unlocking new knowledge regarding ribosome function and protein synthesis, which is crucial for all cellular functions and life itself.

Acknowledgments

I would like to thank my mentor, Dr. Swastik De, for providing me with so many resources for this research project and guiding me every step of the way. With his help, I collected a large sample size to analyze and create 3D volumes. I thank him so much for taking the time to help me with this project. I thank Dr. Joachim Frank for allowing me to access his lab and utilize his resources for this project. His help has been a great factor in its completion and success, and I am very grateful for it.

Table of Contents

List of Figures

Introduction

Background

The translation of stored genetic information into proteins is central to all domains of life. Without this process, organisms cannot function. The eukaryotic ribosome (80S), a complex biomolecular machine composed of the small (40S) and large (60S) subunits, facilitates the reading of sequential codons in messenger RNA (mRNA) by transfer RNA (tRNA), converting this information into the language of amino acids and functional proteins. Without ribosomes, all life would cease to exist, making them an essential molecule to study. With the help of eukaryotic initiation factors (eIFs), the 40S and 60S subunits join together during translation initiation and form a preinitiation complex (PIC). The association of ribosomal subunits is critical for translation initiation, the first stage of protein synthesis, as protein synthesis requires the assembly of the large and small ribosomal subunits (Figure 1).

Figure 1

Protein Synthesis

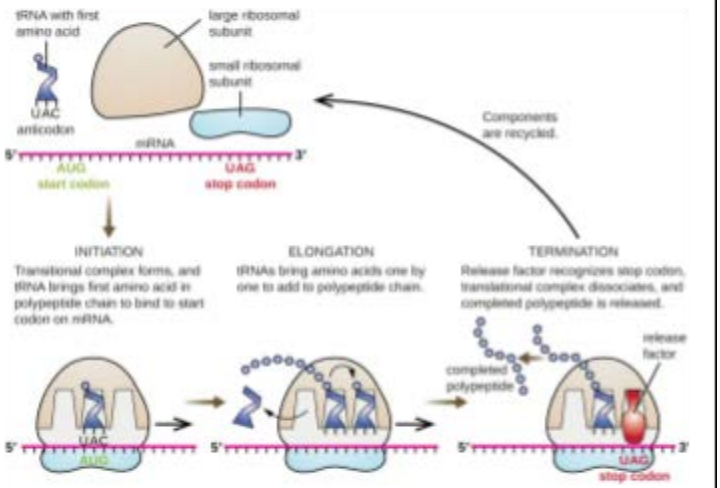

Note. Above is a schematic diagram of protein synthesis. The large and small subunit join together to create a protein based on mRNA sequences. From Miller, C. (2020, September 1). *5.7 protein synthesis.* Human Biology. https://jwu.pressbooks.pub/humanbiology/chapter/5-6-protein-synthesis/.

Review of Literature

Overview of eIF3 and Translation Initiation

Canonical translation initiation is a complex, multistep process that requires the coordinated activity of multiple eIFs with both 40S and 60S ribosomes. Eukaryotic initiation factor 3 (eIF3) is the largest and most complex eIF. It is required for the assembly of the 43S PIC, which contains the 40S subunit, Met-tRNA, and eIF1/1a/2/3; the binding of mRNA to the eIF4F complex; and scanning and AUG recognition (Pestova, 2002). The 43S PIC is then recruited to the cap structure at the 5' end of an mRNA by the eIF4F complex, a group of eIF4 factors, creating the 48S initiation complex (Moore, 2016).

Eukaryotic Ribosomes

Eukaryotic ribosomes (80S) are present in all eukaryotes. This study focuses on the yeast eukaryotic ribosome. Eukaryotic ribosomes consist of a 40S small subunit (SSU) and a 60S large subunit (LSU). The 40S subunit is involved in the building of the preinitiation complex. The subunit can be divided into head, beak, platform, body, shoulder, left foot, and right foot regions (Klinge, 2012). The

interface between the 40S and 60S subunits is called the inter-subunit side of the 40S subunit. The opposite solvent-facing side of the 40S subunit is termed the solvent-exposed side (Figure 2).

Figure 2

80S Ribosomes

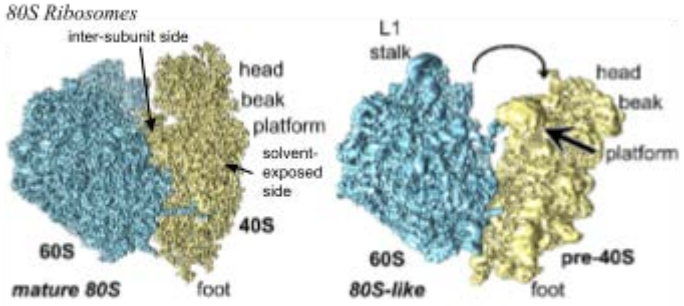

Note. The above figure indicates the head, beak, platform, and foot regions of the 40S subunit and the inter-subunit and solvent-exposed sides. From Rai, J., Parker, M. D., Huang, H., Choy, S., Ghalei, H., Johnson, M. C., Karbstein, K., & Stroupe, M. E. (2020, January 1). An open interface in the pre-80s ribosome coordinated by ribosome assembly factors TSR1 and DIM1 enables temporal regulation of FAP7. bioRxiv. https://www.biorxiv.org/content/10.1101/617910v6.full

Eukaryotic Translation Initiation

Translation initiation is the first stage of protein synthesis. It requires the help of 12 eIFs. It is a multi-step process in which the 40S subunit, methionyl initiator tRNA (Met-tRNA$_i$), and eIFs assemble to form the 43S and 48S preinitiation complexes (PIC). The 40S and 60S subunits are assembled into the 80S initiation complex at the start (AUG) codon of an mRNA and begin the process of protein synthesis from the mRNA's information. Translation initiation is a critical stage, as initiation at the wrong site on the mRNA causes extended, truncated, or out-of-frame translation products (Aitken, 2016).

Eukaryotic Initiation Factor 3 (eIF3)

Eukaryotic translation initiation requires the 40S subunit, 60S subunit, and eIFs (Pestova, 2001). Among these initiation factors, eIF3 is the largest and most complex, with a mass of about 800 kilodaltons (kDa). eIF3 plays a role in translation initiation, termination, ribosomal recycling, and the reading of codons (Valasek, 2012). It is required for the assembly of the 43S preinitiation complex, which contains the 40S subunit, Met-tRNA$_i$, and eIF1/1a/2/3; the binding of mRNA to the eIF4F complex; and scanning and start codon (AUG) recognition (Pestova, 2002). Varying expressions of eIF3 also contribute to different pathological conditions, including cancer and some neurodegenerative diseases (Gomes-Duarte, 2018). As of 2024, eIF3 appears to bind near the mRNA-entry channel of the 40S subunit during initiation to facilitate mRNA binding onto the PIC. At the exit channel, it appears to stabilize the binding of mRNA to the PIC. It also stabilizes the 43S and 48S PIC. However, it is unknown whether these interactions are mediated by all of eIF3's subunits, multi-subunit eIF3 complexes, or individual eIF3 subunits (Ide, 2024).

Yeast eIF3 (yeIF3)

The eIF3 complex consists of 13 subunits, eIF3a-m (des Georges, 2015). It is the only factor that greatly varies in structure between yeast and mammals. The mammalian eIF3 (meIF3) contains all 13 subunits. However, yeIF3 contains only five essential subunits that perform the essential tasks of eIF3 – a/Tif32, b/Prt1, c/Nip1, g/Tif35 and i/Tif34 (Llácer, 2021) – and one nonessential and nonstoichiometric

subunit, j, which associates loosely with the complex (Elantak, 2010; Fraser, 2004; Nielsen, 2006; Valasek, 2001).

yeIF3 Functions in a Dynamic Compositional Equilibrium

Research conducted by the Gonzalez lab studied reconstituted yeast eIF3 in vitro using a new single-molecule light scattering microscopy technique. They found that the full yeIF3 complex does not function as a uniform entity; instead, it is in a dynamic equilibrium with eIF3's subcomplexes and subunits (Ide, 2024). Since yeIF3 functions as different subunits, it is crucial to identify the specific roles of its subunits.

Formation of the PICs During Translation Initiation

The 43S PIC is formed during translation initiation. First, eIF1, 1A, and 3 bind to the 40S subunit. These eIFs help recruit Met-tRNA$_i$ as a ternary complex (TC) with eIF2-GTP. Finally, eIF5 may be recruited with the TC or eIF3 (Llácer, 2021). The 43S PIC is then recruited to the cap structure at the 5' end of an mRNA by the eIF4F complex. eIF4G/eIFiso4G interacts with polA-binding proteins, which enhances the formation of the circular mRNA structure. The structure enables the 43S complex to bind to the mRNA, forming the 48S PIC (Figure 3). The 48S PIC then scans for the first start codon (Moore, 2016).

Figure 3
PICs in Translation Initiation

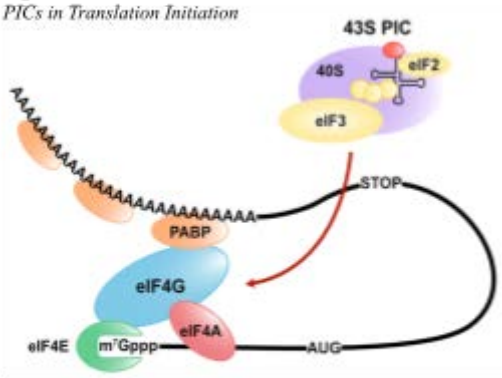

Note. Above is a schematic figure of the binding of the 43S PIC onto the mRNA. From Fukao, A., Tomohiro, T., & Fujiwara, T. (2021, July 6). *Translation initiation regulated by RNA-binding protein in mammals: The modulation of translation initiation complex by trans-acting factors*. MDPI. https://www.mdpi.com/2073-4409/10/7/1711

Previous Research on the Position of yeIF3 in a 48S PIC

In Hinnebusch *et al.,* 2017, researchers achieved structures of the 48S PIC, formed by the 43S PIC, eIF4F, and mRNA. They identified the location of yeIF3 domains in the 48S complex. They conclude that the yeIF3a/c and yeIF3b/i/g domains bind near the exit and entry channel opening on the solvent side of the 40S subunit and eIF3b/i/g domains bind near the 40S entry channel so that eIF3 essentially circles the PIC with its different subunits (Figure 4).

Figure 4
yeIF3 in the 48S PIC

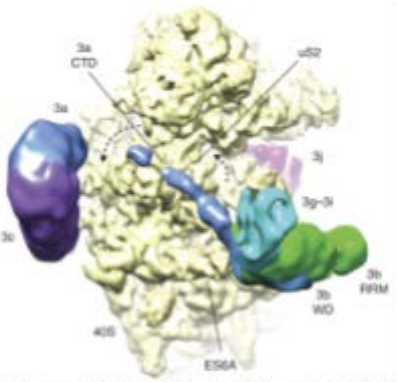

Note. Above presents the findings in Hinnebusch *et al.* regarding yeIF3 binding in the 48S PIC. From Aylett CH et al. *Structure of a yeast 40s-EIF1-EIF1A-EIF3-EIF3J initiation complex*. Nature structural & molecular biology. https://pubmed.ncbi.nlm.nih.gov/25664723/

However, they confirmed that the precise roles of yeIF3 are still unknown because there is a lack of structural information on the factor's location and interactions within the 43S PIC. Additionally, the

complete structure of eIF3 has not yet been determined because of its subunit complexity. The precise roles of the PIC's other factors (eIF1/1a/2) are also hindered by the lack of a high-resolution PIC structure containing these factors (Hinnebusch, 2017).

As of May 2024, there is still no high-resolution structural information about the precise role of yeIF3 in the 43S PIC during translation initiation. The roles of each subunit of yeIF3 (a, b, c, i, g) during translation initiation are still unknown, as there has been no research creating a high-resolution structure of yeIF3's location and interactions within the 43S PIC over the last seven years. This is due to the lack of a data-collection methodology to collect and image the subunits of yeIF3 separately in 43S PIC.

Problem Statement

- The precise binding location and interactions of yeIF3a/c/b/i/g in the 43S PIC are unknown due to a lack of a high-resolution 43S PIC structure.

Objective

- To determine the precise binding location and interactions of yeIF3a/c/b/i/g in the 43S PIC during yeast translation initiation by analyzing modular multicomponent systems of yeIF3 subunits.

Methodology

Role of Student vs. Mentor

Before beginning my research, my mentor prepared grids containing purified yeast ribosome samples with different subunits of eIF3 (a, c, b, i, and g) and stored them in liquid nitrogen. He collected data for 43S complexes with elF3$_{entry}$ (a$_{CTD}$/b/i/g), elF3 full-complex (a/c/b/i/g), eIF3a/c/b, and eIF3b/i/g. He then took microscopic images with a Titan Krios3 microscope. These images were uploaded to my lab computer and transferred to me.

I analyzed these datasets from the lab office and my home through a virtual connection to my lab's computers and servers. Data analysis included motion correction, CTF correction, particle picking, 2D classification, 3D reconstruction, 3D refinement, 3D classification, model building, map fitting, and model analysis. At no point in my research did I handle the ribosome samples or use a microscope, and no tissue samples or human data were used.

Explanation

A novel technique allowed my mentor to purify each subunit separately so that their individual functions could be determined. We have analyzed a modular multicomponent system by collecting and analyzing datasets for elF3$_{entry}$ (a$_{CTD}$/b/i/g), elF3 full-complex (a/c/b/i/g), eIF3a/c/b, and eIF3b/i/g. The datasets were then analyzed using cryo‑electron microscopy single-particle analysis. The following

methodology was performed for all datasets.

Grid Preparation (Mentor Role)

Cryo-EM grids were prepared by the mentor using Holey Carbon gold Quantifoil R1.2/1.3 300-mesh grids. The grids were glow-discharged for 45 seconds in a PELCO easiGlow at 20 mA to ensure optimal sample adhesion. A volume of 3.5 µL of the sample at 250nM concentration was added to the grids, which were then blotted for 3 seconds with a blot force setting of 3 at 26°C and 100% humidity using an FEI Vitrobot Mark IV. The grids were rapidly plunge-frozen in liquid ethane and stored in liquid nitrogen until data collection. The student did not partake in this part of the data collection.

Data Collection (Mentor Role)

Cryo-EM data were collected by the mentor on a Titan Krios3 microscope operating at 300 kV, equipped with a Gatan K3 Summit direct electron detector (DED). Images were recorded in counting mode at a nominal magnification of approximately 105,000×, corresponding to a pixel size of 0.844 Å. Depending on the sample, between 5,000 and 10,000 movies were collected with a total electron dose ranging from 50 to 60 $e^-/Å^2$. Each movie was fractionated into 40 frames with a total exposure time of 2.5 seconds. Automated data acquisition was performed using Leginon software, with a defocus range set between -1.5µm and -2.5µm to optimize contrast and resolution. Real-time processing was used for quality assessment and feedback during data collection.

The images taken from these movies were organized and uploaded onto a computer for image processing. The student performed image processing and data analysis.

Image Processing (Student Role)

CryoSPARC was used to process the images. The micrographs from the acquired data were motion-corrected using the patch motion correction algorithm to minimize the frame-to-frame beam-induced motion of the particles. The images were corrected using Contrast Transfer Function (CTF) Correction, which restored the microscope's initial high-resolution information.

Particle Picking (Student Role)

The motion and CTF-corrected image files from cryoSPARC were uploaded onto cryOLO, and settings were modified to allow for particle picking. A box size of 256 was used to ensure enough data was captured around the particle. Ribosomes were manually picked from these corrected images to train cryOLO's neural network-based particle picker. Visible particles, or ribosomes, were picked from each micrograph until ~5,000 particles were selected to train cryOLO's neural network (Figure 5). The trained model then picked particles, which increased the total number of particles in the dataset. The model was

trained again by manually selecting particles that were missed and deselecting junk picks such as noise, ice, and aggregates. After multiple rounds of training and manual correction, the student was satisfied with the resulting trained model. This trained model was then used to pick around 1,000,000 particles for each dataset. These particles were then extracted.

Figure 5
Particle Picking

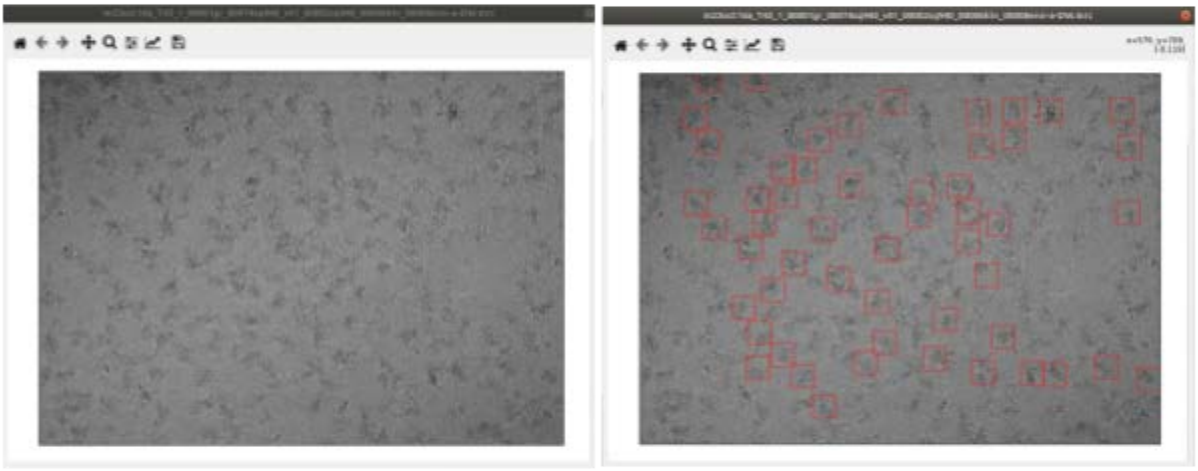

Note. The above figure shows the manual picking process in cryOLO. The image on the right has picked particles, indicated by the red boxes around the particles. (Student generated image)

Classifying Particles (Student Role)

After picking ribosomes and extracting the particles from the images, a 2D classification was run in cryoSPARC. The 2D classification was run to identify incorrectly picked "junk" particles and to classify "good" particles into different classification groups. Around 500,000 "good" particles were kept in each dataset. After the 2D classification, an initial 3D classification was run in cryoSPARC and RELION to identify the major conformational states present in each sample and remove any remaining poor-quality particles. All particles were then re-extracted at a full-size pixel box and processed with 3D refinement, anisotropic magnification correction, refocus refinement, and beam tilt estimation in RELION. After each refinement process, the particles underwent 3D classification in cryoSPARC and RELION to remove any more poor-quality particles and were checked for an increase in resolution and visual improvement of map quality. Once the refinements in RELION did not improve the map quality, the student used all frames to perform particle polishing and completed the refinement process again. Focused classification on consensus maps was performed to isolate the ribosomes' desired confirmation or compositional states.

Model Building (Student Role)

3D volumes of the 40S yeast subunit were then created from the 2D and 3D classifications to visualize yeIF3 on the 40S subunit. Initial model building was performed using ChimeraX, RELION 4, and Coot. All models underwent one round of Phenix geometry minimization to idealize the models' geometry according to standard geometry restraints and multiple rounds of Phenix real-space refinement to refine the models into maps. These model validations ensure the volumes and models do not break any laws of physics or chemistry.

Map Fitting (Student Role)

The models were then used to perform map fitting in ChimeraX using its "fit in map" tool to isolate eIF3-containing particles (Figure 6). Focused classification strategies were employed, utilizing masks targeted at distinct peripheral regions of the 43S complex. Multiple masks were designed, including the eIF3b- and eIF3b/i/g-solvent side (3b-s and 3b/i/g-s) masks, a TC with eIF3b/i/g-solvent side (TC3big-i) mask, and eIF3b- or eIF3b/i/g-intersubunit side (3b-i or 3big-i) masks, as well as a TC mask derived from previously published structures (refs: 6GSM, 6FYX). Subsequent focused classifications using the TC mask yielded maps facilitating the identification of classes where both TC and specific eIF3 variants were clearly discernible.

Figure 6
Map Fitting

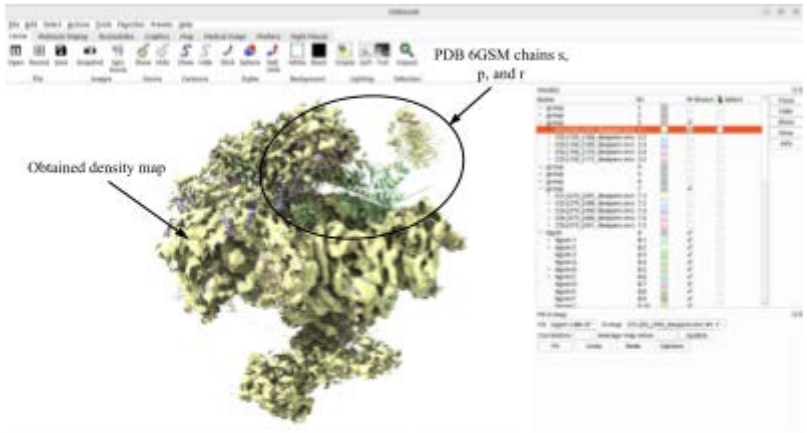

Note. The above figure shows map fitting in ChimeraX. PDB chains are fit into the obtained density maps to visualize the locations of the eIFs. (Student generated image)

CryoDRGN Heterogeneity Analysis (Mentor and Student Role)

CryoDRGN heterogeneity analysis was conducted on all filtered particles to explore how individual eIF3 modules influence ribosome structure, specifically the 40S head and body dynamics. By employing weighted k-means clustering of the heterogeneity landscape, 10, 20, or 30 volumes were extracted for further analysis, which was utilized for investigating head and body dynamics through fitted models.

Equipment and Materials

The cryo-EM data was provided to the student by the mentor to perform image processing and data analysis through a virtual connection to a lab computer. The student used **cryoSPARC** to motion-correct the images to minimize the frame-to-frame beam-induced motion of the particles using the patch motion correction algorithm. To correct the CTF, the cryoSPARC CTF correction algorithm was used, restoring the initial high-resolution information from the microscope. The student also used **cryOLO** to train a neural network to pick ribosomal particles and used cryoSPARC to run 2D and 3D classifications on the particles, discarding the "junk" particles and classifying the good particles. **ChimeraX**, **RELION 4**, and **Coot** were used to model the ribosome from the classifications. **Phenix** was used to idealize the models' geometry according to standard geometry restraints, to refine the models into maps, and to ensure the volumes and model did not break any laws of physics or chemistry. **ChimeraX** was used for map fitting to visualize the subunits of yeIF3 on the 43S PIC. Lastly, **cryoDRGN** was used to determine individual eIF3 modules' influence on ribosome structure.

Results

Full Results

2D Classes

After running 2D classification in cryoSPARC, the following twenty-one "junk" classes were removed. An example of "junk" classes from one dataset is shown in Figure 7. These classes are either noisy particles or particle-picking artifacts. 2D classification classifies the particles into different groups based on their structure in different stages of canonical translation initiation.

Figure 7
Junk 2D Classes

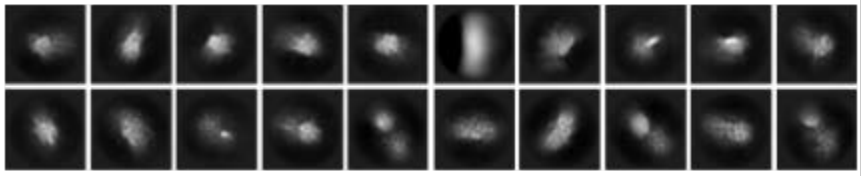

Note. Above shows the "junk" 2D classifications that were removed to sort out the "junk" particles from the particle dataset. (Student generated image)

Thirty "good" 2D classes were grouped from the particle dataset (Figure 8). These classifications showed 2D averages of the selected particles and resulted in images of the yeast 40S

Figure 8
Good 2D Classes

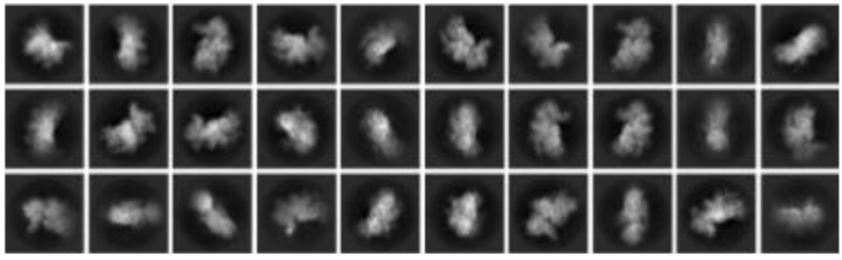

Note. Above shows the good 2D classifications from one dataset. These are images of the ribosomal subunit taken from different angles. (Student generated image)

subunit from different angles. These 2D classifications were used to create 3D volumes of the 40S ribosome.

3D Volumes

Figures 9 and 10 are images of 40S yeast ribosome volumes at 2.79Å. Figure 9 is a sharpened image of the volume. Figure 10 is an unsharpened image of the volume. These volumes show the quality of our reconstruction and the resulting map.

Figure 9
Sharpened 40S Ribosome

Note. Above is a sharpened image of the 40S yeast subunit volume at 2.79Å. (Student generated image)

Figure 10
Unsharpened 40S Ribosome

Note. Above is an unsharpened image of the 40S yeast subunit volume at 2.79Å. (Student generated image)

Multiple 3D volumes were obtained with different resolutions. Figures 11 and 12 indicate the resolutions of two different volumes using the gold standard FSC cutoff of 0.143. The volume in Figure 11 has a resolution of 2.79 Å, so it has a higher resolution than the volume in Figure 12.

Figure 11
GSFSC Resolution

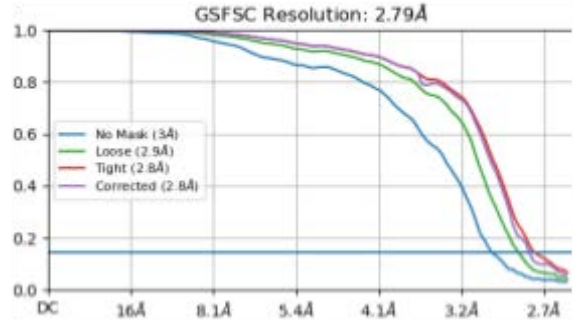

Note. Above is a chart indicating the resolution of the volume at 2.79Å. (Student generated graph)

Figure 12
GSFSC Resolution

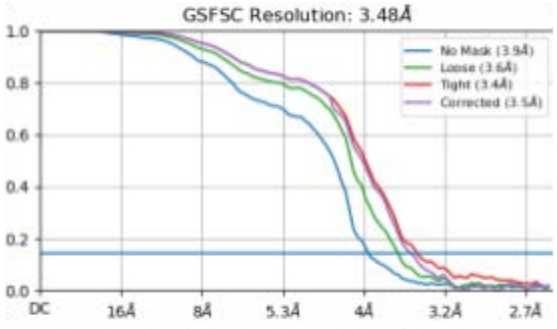

Note. Above is a chart indicating the resolution of the volume at 3.48Å. (Student generated graph)

Figure 13 contains another 3D volume of the 40S yeast ribosome at 5.3Å. The volume was reconstructed using Coot, RELION 4, and ChimeraX. The blue points around it indicate that a particle image was used to form the volume from that projection or angle. All of the particles and projections together form the entire 3D volume. Red sections indicate that more projections were used from that angle of the volume.

Figure 13
3D Volume Construction

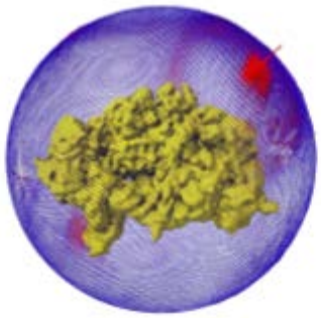

Note. Above shows the angles used to create the 5.3Å 3D volume of the 40S yeast subunit. (Student generated image)

Figure 14 shows the obtained volumes for yeIF1, 1A, 3a/c, 3b, 3i/g, the TC, and the 40S subunit obtained through classifications.

Figure 14
3D Volumes of yeIFs and 40S Subunit

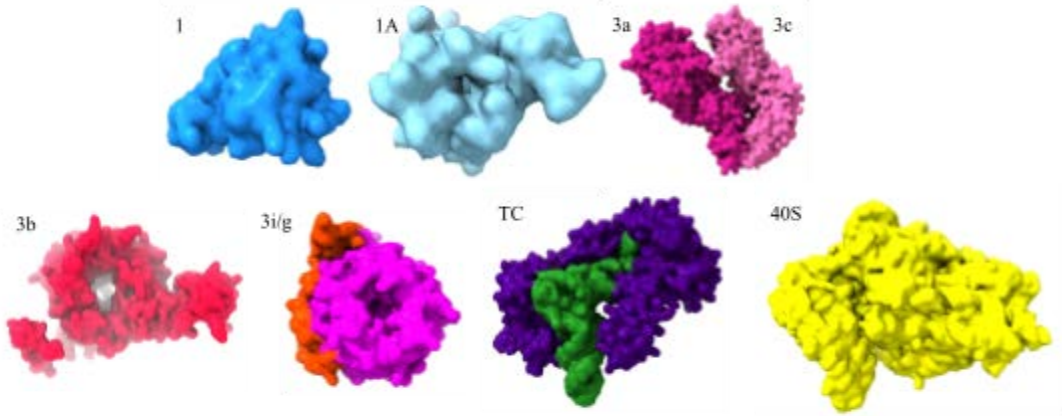

Note. The above figure shows the resulting 3D volumes of yeIF1, 1A, 3a/c, 3b, 3i/g, the TC, and the 40S subunit. (Student generated image)

3D Models With Fitted Maps

Proposed Models for eIF3b/i/g Relocation After mRNA Binding.

Figure 15 shows our proposed binding of the elF3 reconstituted full-complex (a/c/b/i/g) dataset during canonical translation initiation. These models with fitted maps were created from the eIF3 reconstituted full-complex dataset. The binding of this complex is comparable to the binding of native eIF3. eIF3b/i/g binds to both sides of the 40S in the elF3 full-complex. The 43S PIC is able to bind based on a gel-based equilibrium binding assay. According to a gel-based equilibrium mRNA recruitment assay, mRNA is able to be recruited and bound to the 43S PIC.

Figure 15

Proposed Models for eIF3b/i/g Relocation After mRNA Binding

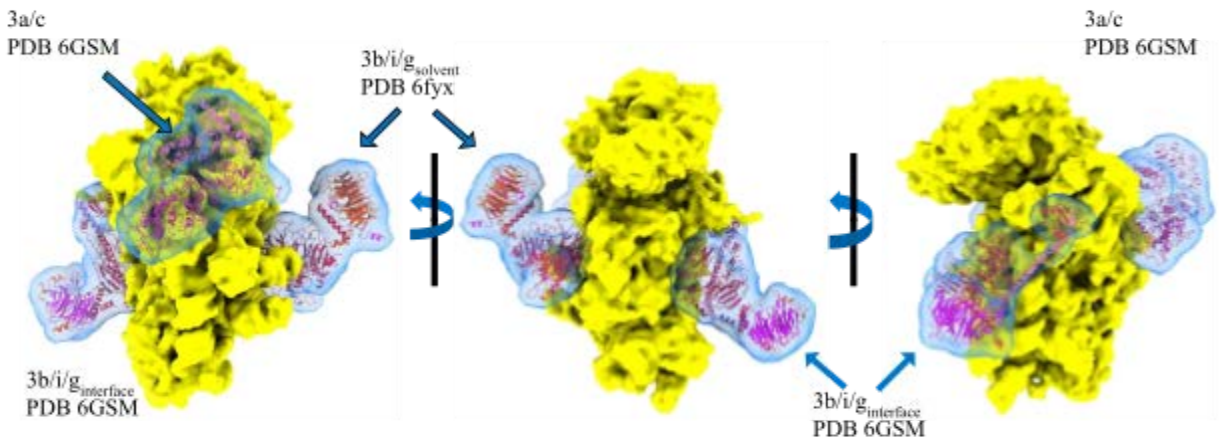

Note. Above shows our proposed binding of the eIF3 full-complex (a/c/b/i/g) during canonical translation initiation. eIF3b/i/g binds to both sides of the 40S in the eIF3 full-complex. The 43S PIC is able to bind, and mRNA is later able to be recruited and bound to the 43S PIC. (Student generated image)

eIF3b/i/g Binds to Both Sides of the 40S Subunit in the Absence of mRNA.

Figure 16 shows the binding location of eIF3b/i/g in the same dataset, eIF3 reconstituted full-complex, at a resolution of 7.7Å. This model was created from 48,385 particles. It has comparable binding to native eIF3, as eIF3b/i/g is able to bind to both sides of the 40S in the absence of mRNA. The 43S PIC is able to bind, and mRNA is later able to be recruited and bound to the 43S PIC.

Figure 16

eIF3b/i/g Binds to Both Sides of the 40S Subunit in the Absence of mRNA

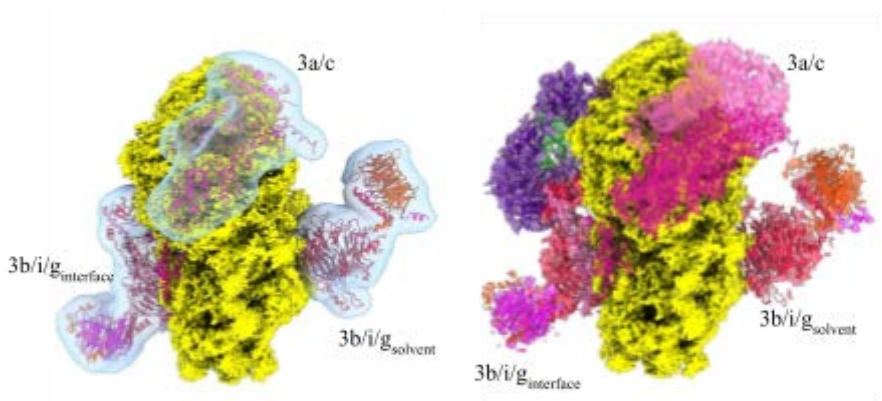

Note. The above model has a resolution of 7.7Å and was created from 48,385 particles. It shows the binding location of eIF3b/i/g on both sides of the 40S in the absence of mRNA in the eIF3 reconstituted full-complex, which has comparable binding to native eIF3. The 43S PIC is able to bind, and mRNA is later able to be recruited and bound to the 43S PIC. (Student generated image)

eIF3a/c is not Essential for the Binding of eIF3b/i/g to the 40S.

The resulting model with fitted maps from our eIF3b/i/g dataset reveals that eIF3a/c is not essential for the binding of eIF3b/i/g to the yeast 40S subunit (Figure 17). It was created from ~130k particles and has a resolution of 4Å. eIF3b/i/g was able to bind poorly to the 40S subunit in the absence of

the eIF3a$_{CTD}$. eIF3a$_{CTD}$ is the C-terminal region of eIF3a that promotes mRNA recruitment and scanning. The 43S PIC cannot bind, and mRNA cannot be recruited to the ribosome due to the lack of the C-terminal.

Figure 17

eIF3a/c is not Essential for the Binding of eIF3b/i/g to the 40S

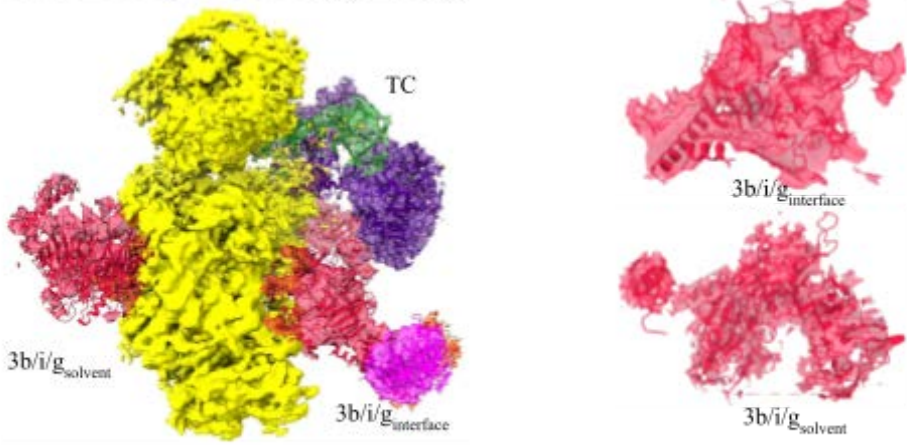

Note. The following model was created from ~130k particles and had a resolution of 4Å. It shows that eIF3b/i/g binds poorly to the 40S ribosome in the absence of eIF3a$_{C\text{-}term}$. The 43S PIC could not bind, and mRNA could not be recruited to the ribosome. (Student generated image)

Entry Channel Module eIF3a$_{CTD}$/b/i/g is Sufficient for 40S Binding.

Figure 18 shows the resulting model of the eIF3$_{entry}$ dataset, which contained eIF3a$_{CTD}$/b/i/g. These subunits were sufficient to bind to the 40S subunit. The binding of eIF3b/i/g was similar to that of the eIF3 reconstituted full-complex dataset, as eIF3$_{entry}$ showed the presence of eIF3b/i/g on both sides of the 40S subunit. The 43S PIC is able to bind, and mRNA is slowly recruited to the ribosome roughly four times slower than the fully reconstructed eIF3.

Figure 18

Entry Channel Module eIF3a$_{CTD}$/b/i/g is Sufficient for 40S Binding

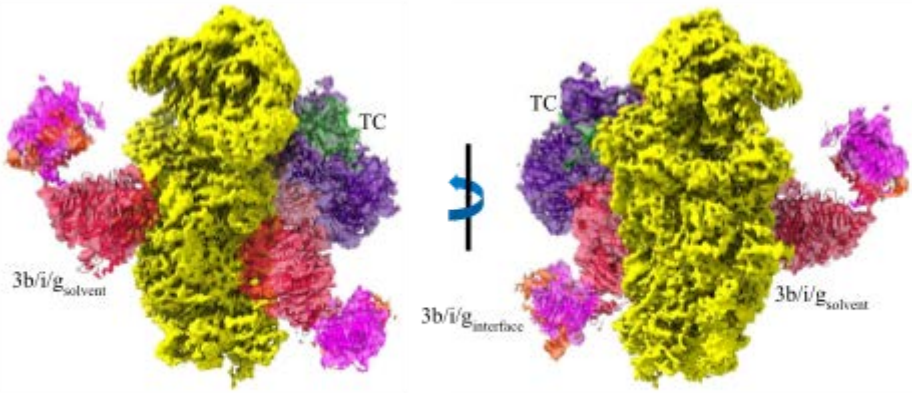

Note. Above shows the resulting model of the eIF3$_{entry}$ dataset. These subunits were able to bind to the 40S subunit. The binding of eIF3b/i/g was similar to that of the eIF3 reconstituted full-complex dataset, as eIF3$_{entry}$ showed the presence of eIF3b/i/g on both sides of the 40S subunit. The 43S PIC is able to bind, and mRNA is recruited to the ribosome but at a 4x slower rate than the fully reconstituted eIF3. (Student generated image)

eIF3b Can Bind to the 40S in the Absence of eIF3i/g.

Figure 19 shows the models that resulted from the dataset with eIF3a/c/b. This model had a resolution of 5.7Å and was created from 80,103 particles. eIF3b is able to bind to the 40S subunit without the presence of eIF3i/g. The PIC is able to bind, but mRNA is not recruited to the ribosome.

Figure 19

eIF3b Can Bind to the 40S in the Absence of eIF3i/g

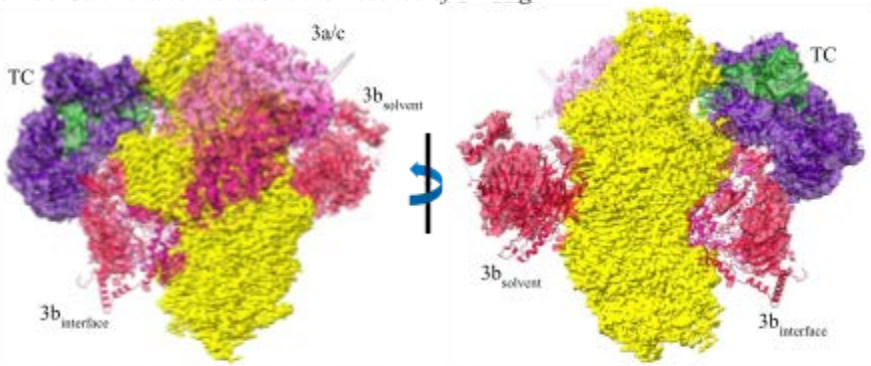

Note. The above model from the eIF3a/c/b dataset had a resolution of 5.7Å and was created from 80,103 particles. eIF3b is able to bind to the 40S subunit without the presence of eIF3i/g. The PIC is able to bind, but mRNA is not recruited to the ribosome. (Student generated image)

eIF3a/c Helps Stabilize the 40S Head.

Figure 20 shows three datasets: eIF3 reconstituted (subunits a, c, b, i, and g), eIF3a/c/b, and $eIF3_{entry}$ (subunits a_{CTD}, b, i, and g). Datasets eIF3a/c/b and eIF3 reconstituted show that eIF3a/c stabilizes the head of the 40S subunit, as the $eIF3_{entry}$ dataset (without eIF3a/c) showed more motion than the other two datasets. The PIC is able to bind, but mRNA is not recruited to the ribosome.

Figure 20

eIF3a/c Helps Stabilize the 40S Head

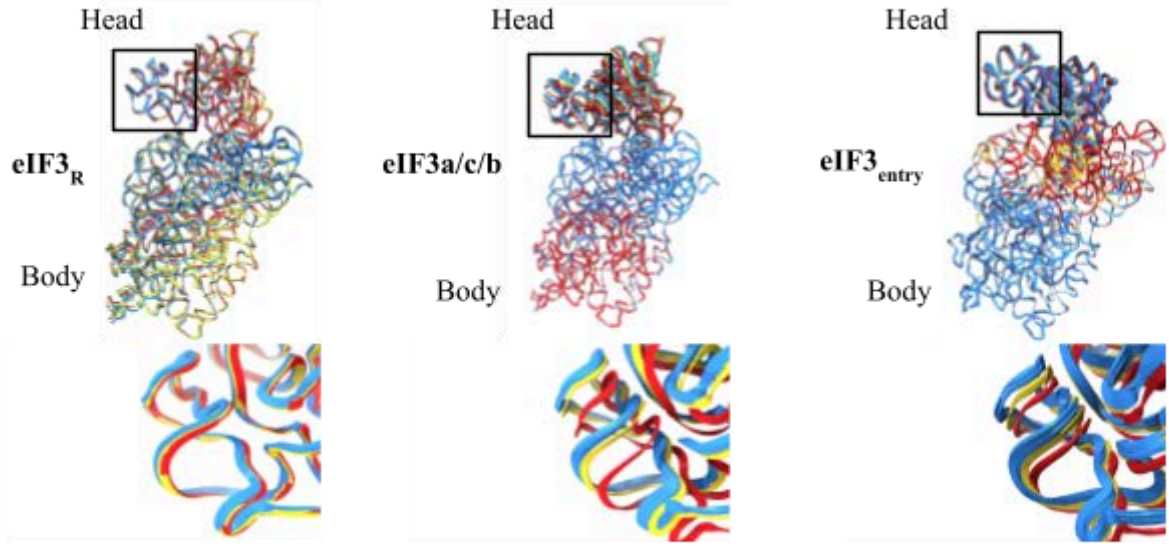

Note. The above figure shows the 40S subunit for three datasets: eIF3 reconstituted (subunits a, c, b, i, and g), eIF3a/c/b, and $eIF3_{entry}$ (subunits a_{CTD}, b, i, and g). eIF3a/c stabilizes the head of the 40S subunit. The PIC is able to bind, but mRNA is not recruited to the ribosome. (Student generated image)

Discussion

Analysis of Data

Our goal to determine the precise binding location and interactions of yeIF3a/c/b/i/g in the 43S PIC during yeast translation initiation by analyzing modular multicomponent systems of yeIF3 subunits was achieved. We have obtained high-resolution 3D reconstructions of yeIFs and the yeast 40S subunit. Our models identify the functions and binding locations of yeIF3a/c/b/i/g during yeast canonical translation initiation.

No statistical tests were performed because variables were not studied.

eIF3b Can Bind to Both Sides of 40S Even in the Absence of mRNA

Following rigorous 2D classification, we applied 3D classification using the eIF3b-i and -s masks, reconstructing the resultant classes to achieve resolutions ranging from 6 to 8 Å (Figure 16). Notably, nearly all $eIF3_{full}$ classes displayed well-resolved eIF3a/c near the exit channel, consistent with previously reported 48S structures. Although eIF3b was less well-resolved, it remained identifiable on both the solvent and interface sides of the 40S subunit, which was also consistent with previously reported 48S structures.

Structurally, these densities are consistent with earlier findings, but we were surprised to detect eIF3b on both sides of the 40S subunit despite the absence of mRNA in our complexes. Focusing on the TC for masked 3D classification, we consistently obtained classes with eIF3b densities on both faces of the 40S, alongside improved tRNA coverage, sometimes within the same volume. However, eIF3i/g remained elusive and poorly resolved in our maps.

To investigate the dual appearance of eIF3b in 43S complex maps, we conducted additional classifications to determine if this resulted from a mixture of particles with eIF3b on opposite sides of the 40S. However, despite extensive focused and multi-class classification attempts, we failed to isolate classes exhibiting eIF3b exclusively on one side. Notably, the relatively weak density of eIF3b compared to ribosomal components implies conformational flexibility, suggesting that this subunit adopts multiple configurations within the 43S complex.

The Entry Channel Module Can Bind to the 40S Subunit By Itself and Shows Binding to Both Sides of the 40S Subunit

3D classification of the 43S complex containing $eIF3_{entry}$ with the eIF3b-s mask revealed multiple classes with eIF3b bound to the solvent side of the 40S subunit. One such classification is shown in Figure 18. Some classes also showed eIF3b on the intersubunit side, which is consistent with our previous

results. Classification using only a TC mask resulted in classes where both the ternary complex and eIF3b-s were resolved. However, when the eIF3b-i mask was applied, the resulting classes displayed only weak eIF3b densities there. Using a mask that included both eIF3b-s and -i, we observed classes with either the ternary complex alone or the ternary complex along with eIF3b on both sides. Overall, eIF3b was detected on both sides of the 40S, regardless of the mask used, with slightly better coverage for the eIF3b-s side. Additionally, as in previous analyses, eIF3i and eIF3g remained poorly resolved, although faint densities corresponding to their expected locations were consistently observed, independent of the masking strategy employed.

eIF3i/g Depletion Impairs eIF3b Interface Binding, But Not 40S Subunit Association

To investigate the role of eIF3 subunits i and g in mRNA recruitment, we generated an eIF3i/g-deleted version of eIF3 and assessed its activity (dataset eIF3a/c/b). Notably, 3D classification with the eIF3b-s mask revealed classes with well-defined eIF3b density exclusively on the solvent side, while only very weak eIF3b density was observed on the intersubunit side. This is shown in Figure 19. Similarly, classification using the eIF3b-i mask showed poor coverage for eIF3b on this face, whereas the solvent side continued to exhibit better map coverage. When using the TC mask, we identified a class that displayed well-resolved TC, eIF1A, eIF3a, eIF3c, and eIF3b-s, including part of the C-terminal fragment of eIF3a and the N-terminal domain of eIF3c. Remarkably, residues 814-835 of the eIF3a C-terminal domain were well-resolved, forming specific interactions with eIF3b and the h21 es6c region of 18S rRNA. These interactions could be mapped to eIF3a residues 814-823, eIF3b residues 580-590, and h21 es6c residues 666-670. Another class containing 263,261 particles at 4.8 Å resolution showed TC, a poorly resolved eIF1A, and partially disordered eIF3b-i, along with a noisy eIF3b-s. The density differences between the eIF3b-s and eIF3b-i sides across all classes are large enough to suggest that eIF3b favors binding to the solvent side of the 40S subunit in the absence of eIF3i/g. Our maps, in the absence of eIF3i/g, clearly confirm the binding site of eIF3b on the 40S, further validating their density assignment and modeling accuracy.

eIF3a/c's Presence Increases the Stability of the 40S Subunit Head

We conducted cryoDRGN heterogeneity analysis on all filtered particles to explore how individual eIF3 modules influence ribosome structure, specifically the 40S head and body dynamics. By employing weighted k-means clustering of the heterogeneity landscape, we extracted 10 maps for further analysis, which were utilized for investigating head and body dynamics through fitted models.

Figure 20 shows the reconstruction from the $eIF3_{full}$ complex particles displayed very minimal 40S subunit head movement. In contrast, in the presence of only the entry channel module, the 40S

showed three distinct clusters of head positions, with a nearly equal number of particles distributed among them, indicating increased subunit head dynamics. When only eIF3a/c/b is present, the 40S showed minimal head movement, resembling the fully reconstituted eIF3 complex. The results show that eIF3a/c subunits play a critical role in stabilizing the 40S head.

Regarding the 40S body dynamics, the fully reconstituted eIF3 sample exhibited notable 40S body movement while the head remained steady. Compared to this, we observed much less 40S body movement for $eIF3_{entry}$ containing 43S. Similar to this, the eIF3a/c/b-containing 43S PIC also showed minimal body movement, highlighting the impact of missing subunits on body dynamics.

Interestingly, the entry channel module containing 43S and the 43S devoid of eIF3i/g both revealed impaired mRNA recruitment abilities either partially or entirely, which could be at least partly a functional consequence of this altered body dynamics. In other words, the 43S complex bound with the complete eIF3 complex exhibits a stable 40S subunit head while allowing 40S body fluctuations, but the removal of specific modules of eIF3 disrupts this pattern, instead leading to distinct head and body dynamics that are not conducive to efficient 48S complex formation.

Challenges

The development of an accurate neural network picker required dozens of training and over 50,000 manual particle picks. One month was spent training a model that could accurately pick a particle dataset of over 1,000,000.

Past Research

Unlike in Hinnebusch et al., where researchers determined the role of yeIF3 in the 48S PIC, we have determined the binding locations of yeIF3a/c/b/i/g in the 43S PIC. Other main differences between our studies are our datasets' compositions, particle-picking methodology, and results. Both studies determined the binding location of yeIF3a/c/b/i/g, though our study determined the specific functions of these subunits in the 43S PIC before mRNA is recruited to the ribosome.

Implications & Applications

We conducted cryo-EM studies to uncover the molecular basis behind the distinct biochemical behaviors observed in various eIF3 variants. We report novel findings on the roles of yeast eIF3's subunits a, c, b, i, and g during canonical translation initiation. These results are hitherto unreported in current literature. Biochemical assays have shown that $eIF3_{full}$ is proficient in both PIC binding and mRNA recruitment, while $eIF3_{entry}$ performs these functions more slowly, and eIFa/c/b is active in 43S PIC binding but inactive in mRNA recruitment. Our fully reconstituted yeast eIF3 system was shown to be

structurally and functionally identical to its native counterpart, and cryo-EM analysis of this 43S PIC complex revealed eIF3b present on both the solvent and interface sides of the 40S subunit.

For $eIF3_{entry}$, our cryo-EM analysis revealed multiple structural classes, with eIF3b positioned on both the solvent and interface sides of the 40S subunit, similar to the $eIF3_{full}$ complex. This positioning suggests that the entry channel module can assemble competent 43S PICs. However, the observed slower mRNA recruitment may result from altered dynamics in the interaction between $eIF3_{entry}$ and the 40S subunit.

In the case of eIF3a/c/b, which can form a stable PIC but cannot recruit mRNA, cryo-EM analysis showed that eIF3b strongly preferred binding to the solvent side of the 40S subunit over the intersubunit side when eIF3i and eIF3g are absent. This structural observation suggests that eIF3i/g is essential for anchoring eIF3b at the 40S-interface side, ensuring the proper positioning needed for TC interaction and mRNA recruitment. Without these subunits, eIF3b's binding on the interface side is unfavorable, causing a conformational shift in the 40S subunit that obstructs mRNA recruitment. These findings highlight the pivotal role of eIF3i/g in maintaining the structural integrity of the 43S complex required for translation initiation.

The analysis of reconstituted 43S PIC particles revealed how critical the dynamics of the 40S subunit are in explaining the biochemical behaviors observed. Fully reconstituted eIF3-containing complexes exhibited minimal movement of the 40S head but visible body movement, which might be essential for effective mRNA recruitment. In contrast, the eIF3 entry channel module displayed substantial head movements with little body movement, correlating with its slower mRNA recruitment due to head instability. The eIF3a/c/b variant, while maintaining a stable head position similar to the fully reconstituted eIF3, lacked the essential body movement that might be required for mRNA recruitment, a deficiency likely compounded by the absence of eIF3i/g, which is crucial for eIF3b positioning on the interface side.

Additionally, eIF3 is involved in many human diseases, including cancer. Researchers currently believe that specific subunits of eIF3 are found to be elevated or reduced in numerous human tumors, and the overexpression of select subunits and the underexpression of others may cause malignant transformation. Therefore, understanding the role of eIF3 subunits in ribosomal translation initiation will increase knowledge of human disease. Furthermore, analyzing yeIF3's subunits separately is essential for fully understanding the structural dynamics of ribosomal translation. Since eIF3 plays a large role in recruiting mRNA to the ribosome, identifying and understanding the binding location of eIF3's subunits

will increase knowledge regarding the interaction between mRNA and the ribosome. Because proteins are necessary for all life functions, our findings on the binding location of eIF3 are essential. Finally, yeast ribosomes are model organisms for all eukaryotes; therefore, identifying the binding locations of eIF3 allows researchers to apply some of the findings to humans as well.

Future Research

Future studies should be directed at exploring the dynamic roles of eIF3 during elongation and re-initiation, as this would further elucidate the multifaceted functions of this essential complex in eukaryotic translation.

Conclusion

Our goal was to determine the precise binding location and interactions of yeIF3a/c/b/i/g in the 43S PIC during yeast translation initiation by analyzing modular multicomponent systems of yeIF3 subunits. This goal was achieved through a cryo-EM Single Particle Analysis methodology and the examination of reconstituted eIF3 through gel-based assays that assess eIF3's role in PIC formation and mRNA recruitment. We have achieved high-resolution 3D reconstructions of yeIFs and the yeast 40S subunit. Our models identify the roles of yeIF3a/c/b/i/g during yeast canonical translation initiation. We observed that eIF3a/c stabilizes the 40S subunit head, thus preparing the ribosome for mRNA recruitment, while $eIF3_{entry}$'s slower function can be attributed to head instability. The eIF3i/g module plays a pivotal role in securing eIF3b on the interface side of the 40S subunit, ensuring proper mRNA recruitment and PIC formation. In the absence of eIF3i/g, the binding of the depleted eIF3 leads to a conformation of the 40S that impairs mRNA recruitment. Our results suggest that eIF3 operates through a modular mechanism that eliminates the need for an extensive repositioning of eIF3b. Our novel findings inform of previously unknown functions regarding yeIF3 in the 43S PIC. Our results show how the coordinated interaction of eIF3 subunits with the 40S ribosome supports efficient initiation. Our findings provide a robust framework for understanding how each module contributes to the overall mechanism of translation. This modular mechanism model, supported by structural and biochemical data, offers a comprehensive explanation of how eIF3's independent yet cooperative subunit interactions guide 43S PIC assembly and mRNA recruitment. As the most complex translation initiation factor, understanding the structure and functions of eIF3 is essential to unlocking new knowledge regarding ribosome function and protein synthesis, which is crucial for all cellular functions and life itself.

References

Agrawal, R. K., Heagle, A. B., Penczek, P., Grassucci, R. A., & Frank, J. (1999). EF-G-dependent GTP hydrolysis induces translocation accompanied by large conformational changes in the 70S ribosome. Nature structural biology, 6(7), 643–647. https://doi.org/10.1038/10695

Aitken, C. E., Beznosková, P., Vlčkova, V., Chiu, W. L., Zhou, F., Valášek, L. S., Hinnebusch, A. G., & Lorsch, J. R. (2016). Eukaryotic translation initiation factor 3 plays distinct roles at the mRNA entry and exit channels of the ribosomal preinitiation complex. eLife, 5, e20934. https://doi.org/10.7554/eLife.20934

Aylett, C.H., Boehringer, D., Erzberger, J.P., Schaefer, T., & Ban, N. (2015). *Structure of a yeast 40s-EIF1-EIF1A-EIF3-EIF3J initiation complex*. Nature structural & molecular biology. https://pubmed.ncbi.nlm.nih.gov/25664723/

Brown, Z. P., Abaeva, I. S., De, S., Hellen, C. U. T., Pestova, T. V., & Frank, J. (2022). Molecular architecture of 40S translation initiation complexes on the hepatitis C virus IRES. The EMBO journal, 41(16), e110581. https://doi.org/10.15252/embj.2022110581

Cheng, Y., Glaeser, R. M., & Nogales, E. (2017). How Cryo-EM Became so Hot. Cell, 171(6), 1229–1231. https://doi.org/10.1016/j.cell.2017.11.016

des Georges, A., Clarke, O. B., Zalk, R., Yuan, Q., Condon, K. J., Grassucci, R. A., Hendrickson, W. A., Marks, A. R., & Frank, J. (2016). Structural Basis for Gating and Activation of RyR1. Cell, 167(1), 145–157.e17. https://doi.org/10.1016/j.cell.2016.08.075

des Georges, A., Dhote, V., Kuhn, L., Hellen, C. U., Pestova, T. V., Frank, J., & Hashem, Y. (2015). Structure of mammalian eIF3 in the context of the 43S preinitiation complex. Nature, 525(7570), 491–495. https://doi.org/10.1038/nature14891

Elantak, L., Wagner, S., Herrmannová, A., Karásková, M., Rutkai, E., Lukavsky, P. J., & Valásek, L. (2010). The indispensable N-terminal half of eIF3j/HCR1 cooperates with its structurally conserved binding partner eIF3b/PRT1-RRM and with eIF1A in stringent AUG selection. Journal of molecular biology, 396(4), 1097–1116. https://doi.org/10.1016/j.jmb.2009.12.047

Frank, J. (2017). Single-particle Cryo-electron Microscopy: The Path Toward Atomic Resolution: Selected Papers of Joachim Frank with Commentaries Book by Joachim Frank. World Scientific.

Fraser, C. S., Lee, J. Y., Mayeur, G. L., Bushell, M., Doudna, J. A., & Hershey, J. W. (2004). The

j-subunit of human translation initiation factor eIF3 is required for the stable binding of eIF3 and its subcomplexes to 40 S ribosomal subunits in vitro. The Journal of biological chemistry, 279(10), 8946–8956. https://doi.org/10.1074/jbc.M312745200

Fukao, A., Tomohiro, T., & Fujiwara, T. (2021). Translation initiation regulated by RNA-binding protein in mammals: The modulation of translation initiation complex by trans-acting factors. MDPI. https://doi.org/10.3390/cells10071711

Gomes-Duarte, A., Lacerda, R., Menezes, J., & Romão, L. (2018). eIF3: a factor for human health and disease. RNA biology, 15(1), 26–34. https://doi.org/10.1080/15476286.2017.1391437

Hinnebusch A. G. (2017). Structural Insights into the Mechanism of Scanning and Start Codon Recognition in Eukaryotic Translation Initiation. Trends in biochemical sciences, 42(8), 589–611. https://doi.org/10.1016/j.tibs.2017.03.004

Ide, N. A., Gentry, R. C., Rudbach, M. A., Yoo, K., Velez, P. K., Comunale, V. M., Hartwick, E. W., Kinz-Thompson, C. D., Gonzalez, R. L., Jr, & Aitken, C. E. (2024). A dynamic compositional equilibrium governs mRNA recognition by eIF3. bioRxiv: the preprint server for biology, 2024.04.25.581977. https://doi.org/10.1101/2024.04.25.581977

Klinge, S., Voigts-Hoffmann, F., Leibundgut, M., & Ban, N. (2012). Atomic structures of the eukaryotic ribosome. Trends in biochemical sciences, 37(5), 189–198. https://doi.org/10.1016/j.tibs.2012.02.007

Llácer, J. L., Hussain, T., Dong, J., Villamayor, L., Gordiyenko, Y., & Hinnebusch, A. G. (2021). Large-scale movement of eIF3 domains during translation initiation modulate start codon selection. Nucleic acids research, 49(20), 11491–11511. https://doi.org/10.1093/nar/gkab908

Llácer, J. L., Hussain, T., Saini, A. K., Nanda, J. S., Kaur, S., Gordiyenko, Y., Kumar, R., Hinnebusch, A. G., Lorsch, J. R., & Ramakrishnan, V. (2018). Translational initiation factor eIF5 replaces eIF1 on the 40S ribosomal subunit to promote start-codon recognition. eLife, 7, e39273. https://doi.org/10.7554/eLife.39273

Miller, C. (2020). 5.7 protein synthesis. Human Biology. https://jwu.pressbooks.pub/humanbiology/chapter/5-6-protein-synthesis/

Moore P. B. (2009). The ribosome returned. Journal of biology, 8(1), 8. https://doi.org/10.1186/jbiol103

Moore, M., Gossmann, N., & Dietz, K. J. (2016). Redox Regulation of Cytosolic Translation in Plants.

Trends in plant science, 21(5), 388–397. https://doi.org/10.1016/j.tplants.2015.11.004

Nielsen, K. H., Valásek, L., Sykes, C., Jivotovskaya, A., & Hinnebusch, A. G. (2006). Interaction of the RNP1 motif in PRT1 with HCR1 promotes 40S binding of eukaryotic initiation factor 3 in yeast. Molecular and cellular biology, 26(8), 2984–2998. https://doi.org/10.1128/MCB.26.8.2984-2998.2006

Pestova, T. V., Kolupaeva, V. G., Lomakin, I. B., Pilipenko, E. V., Shatsky, I. N., Agol, V. I., & Hellen, C. U. (2001). Molecular mechanisms of translation initiation in eukaryotes. Proceedings of the National Academy of Sciences of the United States of America, 98(13), 7029–7036. https://doi.org/10.1073/pnas.111145798

Pestova, T. V., & Kolupaeva, V. G. (2002). The roles of individual eukaryotic translation initiation factors in ribosomal scanning and initiation codon selection. Genes & development, 16(22), 2906–2922. https://doi.org/10.1101/gad.1020902

Rai, J., Parker, M. D., Huang, H., Choy, S., Ghalei, H., Johnson, M. C., Karbstein, K., & Stroupe, M. E. (2020). An open interface in the pre-80s ribosome coordinated by ribosome assembly factors TSR1 and DIM1 enables temporal regulation of FAP7. bioRxiv. https://www.biorxiv.org/content/10.1101/617910v6.full

Valásek, L., Hasek, J., Nielsen, K. H., & Hinnebusch, A. G. (2001). Dual function of eIF3j/Hcr1p in processing 20 S pre-rRNA and translation initiation. The Journal of biological chemistry, 276(46), 43351–43360. https://doi.org/10.1074/jbc.M106887200

Valásek L. S. (2012). 'Ribozoomin'--translation initiation from the perspective of the ribosome-bound eukaryotic initiation factors (eIFs). Current protein & peptide science, 13(4), 305–330. https://doi.org/10.2174/138920312801619385